Wind Energy

WILEY

RESEARCH ARTICLE OPEN ACCESS

Scaled Physical Modelling of Floating Offshore Wind Turbines Using a Neural Network-Based Surrogate Model for Aerodynamic Emulation

Emma C. Edwards[1,2] | Edward Barbour[3,4] | Tom Tosdevin[2] | Edward Ransley[2] | Kieran Monk[2] | Alastair Reynolds[2] | Anna Holcombe[2] | Scott Brown[2] | Deborah Greaves[2] | Martyn Hann[2]

[1]Department of Engineering Science, University of Oxford, Oxford, UK | [2]School of Engineering, Computing and Mathematics, University of Plymouth, Plymouth, UK | [3]Centre for Renewable Energy Systems Technology, Loughborough University, Loughborough, UK | [4]Birmingham Energy Institute and School of Chemical Engineering, University of Birmingham, Birmingham, UK

Correspondence: Emma C. Edwards (emma.edwards@eng.ox.ac.uk)

Received: 13 June 2024 | **Revised:** 16 April 2025 | **Accepted:** 21 July 2025

Funding: This research was supported by the European Regional Development Fund, grant/award number: O5R19P03188 (Cornwall FLOW Accelerator Project) and the Engineering and Physical Sciences Research Council, UK, grant/award number: EP/T004177/1 ('Extreme Loading on Floating Offshore Wind Turbines (FOWTs) under Complex Environmental Conditions') and EP/S000747/1 ('Supergen ORE Hub').

Keywords: artificial neural network | floating offshore wind | physical modelling | real-time hybrid method | software-in-the-loop

ABSTRACT

Scaled physical modelling of floating offshore wind turbines is a crucial step in the continued development of floating offshore wind to reach Net-Zero goals. However, it is an inherently difficult task due to the incongruity between Reynolds scaling (important for wind effects) and Froude scaling (important for wave effects). One option to overcome this difficulty is to use a real-time hybrid testing approach, whereby a Froude-scaled model is tested in a wave basin with a thruster replacing the wind turbine. Typically, a low-fidelity numerical model is run in real time to determine the appropriate aerodynamic thrust applied by the thruster. In this paper, the real-time hybrid testing approach is extended by using a surrogate model, pretrained on numerical simulations, to determine aerodynamic thrust in the lab. It is found that for less complex wind load conditions, such as constant wind or turbulent wind with the wind turbine controller turned off, multiple linear regressions are satisfactory surrogate models, but for turbulent wind with the wind turbine controller turned on, artificial neural networks offer significant improvement. The development of the appropriate surrogate models is presented, and they are shown to predict thrust on a testing dataset with a mean absolute error over average thrust of $<2\%$ for operational environmental conditions and $<6\%$ for the most extreme environmental conditions tested. The methodology is demonstrated by testing a 1:70 scale of the VolturnUS-S platform with the 15MW IEA wind turbine, in the COAST Laboratory, University of Plymouth, in benign and extreme weather conditions representative of a location in the Celtic Sea. The novel methodology represents an improvement on the ability to accurately test floating offshore wind turbines in the laboratory, by enabling aerodynamics to be represented using higher fidelity numerical modelling, physical or field data.

1 | Introduction

Eighty percent of the global practical offshore wind resource is located in water deeper than 60 m [1]. At these water depths, traditional 'fixed' structures designed to hold offshore wind turbines, which are drilled into the seabed, are infeasible, and therefore, floating platforms become necessary. As a consequence, floating offshore wind turbines (FOWTs) form a major component of the Net-Zero goals in many countries, and it is anticipated that they will make up 13% of global offshore wind capacity by 2050 [1]. However, there is currently only 188 MW of global FOWT capacity installed [2–4]. Hence, a massive upscaling in FOWT deployment will be necessary. A crucial technical challenge to the development of floating offshore wind is scaled physical modelling of FOWTs in a laboratory. Scaled modelling allows for investigation and verification of how FOWTs perform and is crucial for testing aspects of the system such as operational performance and survivability. Furthermore, physical modelling allows for comparison to and verification of novel numerical models. Scaled modelling of a FOWT is an inherently difficult task, due to the scaling discrepancy between Froude scaling (important for the wave effects on the floating platform) and Reynolds scaling (important for wind effects on the turbine and tower). As discussed in the recent review on the state-of-the-art in physical modelling of FOWTs by Otter et al. [5], there are two main methods to overcome this scaling challenge. In the first method, a scaled turbine is used, and either a Froude-scaled rotor is combined with a higher-than-Froude-scaled wind velocity (e.g., Skaare et al. [6], Mortensen et al. [7]) or geometrically modified low-Reynolds ('performance-matched') blades are combined with a Froude-scaled wind velocity (e.g., Goupee et al. [8], Bredmose et al. [9]). In the second method, called real-time hybrid testing (RTHT), first developed by Azcona et al. [10], aerodynamic forces on the turbine and tower are emulated using an actuator or thruster system instead of a scaled rotor. RTHT uses a numerical model to determine aerodynamic forces based on real-time measurement of appropriate experimental parameters (e.g., platform motion) and user-defined simulated wind field. This method removes the need for a scaled turbine and blown wind in the lab. Experiments use either a dynamic cable winch actuator (e.g., Sauder et al. [11]) or a thruster (propeller actuator). While some methods emulate more components of the aerodynamic load (e.g., Otter et al. [12], Urbán and Guanche [13]), most studies concentrate on producing correctly scaled aerodynamic thrust only, since this is generally much larger than gyroscopic force and other out-of-plane forces and more influential to global motion.

In most RTHT systems, to enable real-time calculation of aerodynamic thrust (and/or other forces), a low-fidelity numerical simulation is run in synchronicity with the experiments. Generally, the use of high-fidelity numerical models in such systems is impossible due to practical computational constraints (i.e., the numerical model must be able to respond as close to real time as possible). However, the use of low-fidelity numerical models limits the accuracy of the results, particularly for more extreme loading and responses. In Ransley et al. [14], a new method is proposed whereby a surrogate model is used to determine aerodynamic thrust for a constant wind speed with a fixed blade pitch and rotor speed. In this method, ahead of the laboratory tests, a numerical model is run and a surrogate model is trained on the results, using only input parameters that can be measured in the lab (e.g., platform motions, velocities and accelerations) or user-defined (e.g., wind speed and controller parameters). During the laboratory tests, the surrogate model is then used in place of a numerical model. Therefore, using the measured experimental values and simulated wind as inputs, the aerodynamic thrust is calculated by the surrogate model close to real-time, and a thruster is used to realise the force.

In the present paper, the methodology is extended to enable a more complicated wind loading case to be tested in the lab—a turbulent wind time series with the wind turbine controller activated—and to explore alternative surrogate model techniques. It is shown that lower complexity machine learning models, such as multiple linear regressions (MLRs), are sufficient to accurately calculate the thrust with constant wind speed or a turbulent wind time series with the controller turned off. However, a higher complexity surrogate model, herein a multilayer feedforward artificial neural network (ANN) with carefully engineered features, is needed for the more complex wind load of a turbulent wind speed with the controller turned on.

Surrogate models have been extensively used in engineering in recent times, most commonly for simulation acceleration, optimisation and expanded design-space search. The general concept is that the dynamics of a highly complex system can be approximated with sufficient accuracy by a pretrained model able to run very quickly. Surrogate modelling has had considerable success in aerodynamic simulation, as covered by Sun and Wang [15]. In this area, surrogate models (such as ANNs) are predominantly used to aid optimisation, whereby models are trained on complex, nonlinear and time-consuming aerodynamic simulations and then used for rapid exploration of design spaces. Machine learning methods have also been used to predict the response of floating structures in wave tank experiments [16].

The overall aim of this methodology is to enable surrogate models of higher fidelity numerical models to replace lower fidelity numerical models during RTHT experiments. However, the approach developed is not limited to data generated in numerical models. Data generated through physical measurements, field data, or from digitally twinned systems could also be used if available. In this proof-of-concept study, the methodology is developed using a midfidelity numerical model (OpenFAST [17]) to train appropriate surrogate models for different wind loading cases. The methodology is applied to test a 1:70 scale model of the VolturnUS-S platform [18] with the 15MW IEA wind turbine (IEA-15-240-RWT [19]) in the COAST laboratory at the University of Plymouth. In these laboratory tests, design load case (DLC) 1.6 [20], which represents a 1-in-50-year storm for rated wind speed, is simulated, as well as a benign operational sea-state (DLC 1.1) [20]. These are both modelled in the Celtic Sea in an area marked for FOWT development, off the Southwest coast of the United Kingdom.

The paper is structured as follows. In Section 2, the surrogate modelling problem is formulated, and the solution developed herein is presented. Two types of machine learning algorithms for the surrogate models are developed (namely MLR and ANN), dependent on the complexity of the wind load. Error quantification of the fit of the surrogate models to the numerical models is discussed. In Section 3, the laboratory setup is explained, including instrumentation used. Results from the lab tests are shown and discussed in Section 4. In Section 5, the methodology is discussed, including limitations and lab errors. Finally, in Section 6, conclusions are drawn and possible avenues to improve the methodology are suggested.

2 | Machine Learning Models for Aerodynamic Thrust Prediction

2.1 | Site Selection and Environmental Conditions

The Celtic Sea, which is the region of sea between Southwest England (Cornwall and Devon), Wales and Ireland, has been identified as a target location for floating offshore wind [21]. Therefore, the experiments in this study were carried out to simulate Celtic Sea environmental conditions. Shown in Figure 1a, the chosen site is near the proposed Celtic Sea floating windfarm locations [21], with longitude $= -6.11$ and latitude $= 50.91$.

For FOWT developers, DLC 1.6 [20], which is the 50-year occurrence of rated wind speed (i.e., the 1-in-50 year storm, assuming rated wind speed), is a key test. To select appropriate environmental conditions for this DLC, 42 years of ERA5 hindcast data [22] are used to fit 50-year return period contours of significant wave height, H_s, and peak wave period, T_p, for rated wind speed (U_{mean}=11 m/s), as shown in Figure 1b. A Direct-IFORM approach is used, following Mackay and de Hauteclocque [23]. The normal turbulence model is used, such that turbulence intensity (TI) is set to 15% [20, 24]. Furthermore, a benign, operational sea-state is selected for rated wind speed, to represent a typical sea-state when the turbine is operational (DLC 1.1 [20]). The mean H_s and T_p values from the hindcast data are used to represent this sea-state. These two DLCs are used in this study because they are important for design and certification of FOWTs and also because they represent the most difficult cases to capture sufficiently accurately with a surrogate model due to the nonlinearities of the controller near rated wind.

2.2 | Numerical Simulations of the VolturnUS-S Platform With the 15MW IEA Turbine

To create the training and validation data for the surrogate model, the coupled aero-hydro-servo-elasto numerical model OpenFAST v3.4.1 [17] is used. Github files are used for the VolturnUS-S, a three-column semi-submersible platform [18], with the 15 MW IEA turbine [19, 25] (v1.1). Note that OpenFAST is run at full-scale, assuming 200-m water depth and original mooring setup, as defined in the Github files. The water depth and mooring setup for the experimental setup (defined in Section 3) are different from this reference setup. The purpose of running these simulations was to create sufficient training for a surrogate model for aerodynamic thrust force, which is achievable even with a different water depth and mooring setup, since the physics affecting aerodynamic thrust depends on the turbine movement and incident wind speed, rather than mooring setup or water depth.

To choose the rated wind speed and the corresponding rotor speed and blade pitch values, a sweep of wind speeds is performed with the controller turned on, from 3 to 25 m/s at 0.5 m/s increments, except between 10 and 12 m/s where the increments are reduced to 0.1 m/s. Each windspeed is run for 200 s which is found to be sufficiently long to reach steady-state. The wind speed is specified at the rotor centre, and the wind shear is set to be 0.14 (from IEC 61400-3-1:2019, which is the value given for normal offshore wind conditions [26]). No waves are run, but the platform is allowed to move in six degrees of freedom. From this wind speed sweep, it is found that for the rated wind speed of 11 m/s, the steady-state blade pitch value is 3.17° and the steady-state rotor speed value is 7.56 RPM, which agree well with the reference document [18].

Due to the additional complexities associated with scale modelling of structural behaviour, the system is treated as a rigid body in the numerical modelling, and therefore, tower bending modes are turned off. The inputs to the OpenFAST model, different to the Github files, are wind speed time series,

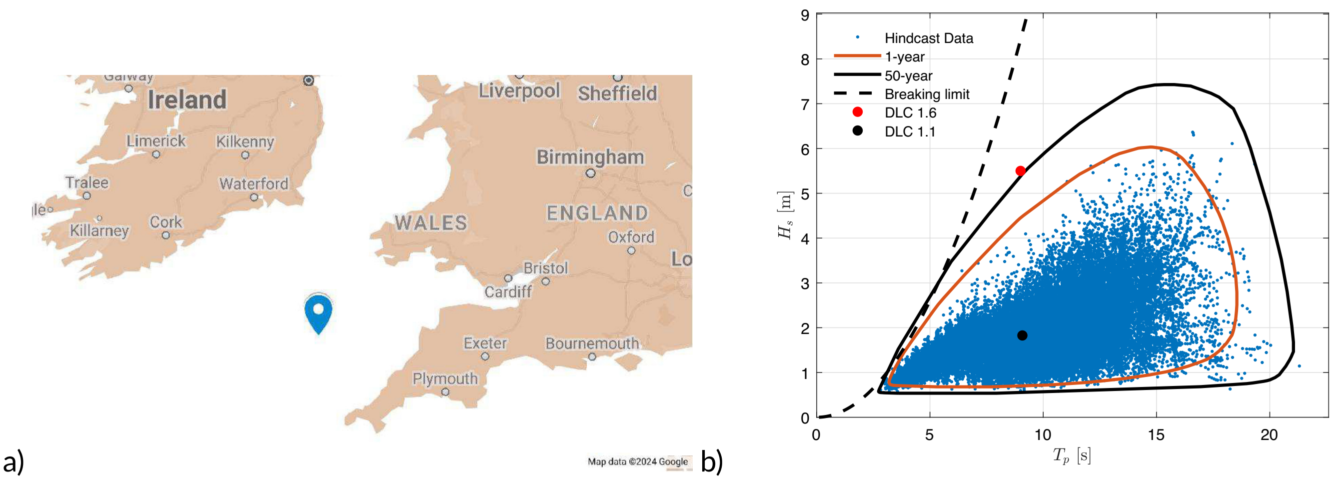

FIGURE 1 | (a) Location of the chosen site to simulate environmental conditions, near the floating wind farm locations proposed by the Crown Estate in the Celtic Sea [21]. (b) Significant wave height, H_s, and peak wave period, T_p, scatter plot for rated wind speed at the chosen site, showing the 50-year contour (solid black curve) and 1-year contour (solid red curve). DLC 1.6 (red dot) corresponds to the '50-year rated' condition, and DLC 1.1 (black dot) corresponds to the 'benign rated' condition.

sea-state (which determines the waves) and the controller parameters. To make the wind time series, the Kaimal turbulence spectra is used [27], for the specified mean windspeed and turbulence intensity, with wind shear always 0.14. The wave time series is determined from the JONSWAP spectrum. The associated full-scale parameters for each run, including mean wind speed (U_{mean}), turbulence intensity (TI), shear, significant wave height (H_s), peak period (T_p), and wave peak enhancement factor (γ) are shown in Table 1. From the simulation, time series of the motions and forces on the system are extracted, with a timestep of 0.025 s. In this study, in the lab, the thrust force is determined by the surrogate model to deliver the correct moment at the base of the tower. Since there is no blown wind, the thruster force accounts for both the aerodynamic thrust force on the rotor and the tower drag due to the incident wind. In OpenFAST, tower drag per length is output for specified nodes along the tower (nodes 1–3, 5 and 7–11 of evenly spaced nodes along the tower height, according to OpenFAST output requirements). Therefore, the force per length is interpolated (quadratic to node 10 and then linear between nodes 10 and 11, due to the tower diameter changing abruptly in the reference Github files for the turbine), multiplied by height from the sea-surface and integrated to give the thruster force required for the equivalent moment at the base of the tower. OpenFAST gives aerodynamic thrust force in the hub coordinate system, which rotates with the blades and is tilted at 6 degrees. Therefore, thrust perpendicular to the tower is calculated as $F_T = F_x \cos(6°) - F_{yz} \sin(6°)$, where $F_{yz} = F_z \cos(\theta) + F_y \sin(\theta)$, where θ is azimuth angle and F_x, F_y and F_z are the aerodynamic forces in the hub coordinate system. Finally, the open-source turbine controller ROSCO [28], which is designed for offshore wind turbines and has Github downloads for the reference turbine and platform (v1.1), is used when the controller is set to 'on'.

The following aerodynamic load cases are run for each of the two sea-state cases (50-year rated and benign rated).

1. **Constant wind, no controller:** This case simulates a constant wind of 11 m/s, with no turbulence intensity, with the ROSCO controller turned off.
2. **Constant wind, with controller:** This case simulates a constant wind of 11 m/s, with no turbulence intensity, with the ROSCO controller turned on. Note that since the body is floating, the apparent wind is variable; hence, the controller is still relevant.
3. **Turbulent wind, no controller:** This case simulates turbulent wind (TI=15%), with the ROSCO controller turned off.
4. **Turbulent wind, with controller:** This case simulates turbulent wind (TI=15%), with the ROSCO controller turned on.

All eight cases (four for each of the two sea-states) are summarised in Table 1. OpenFAST runs are completed for all eight cases. Furthermore, three additional OpenFAST runs are conducted. Firstly, there is a known tendency for underprediction of platform motions in OpenFAST, especially for more extreme waves and for low-frequency responses [29, 30]. To provide representative training data for the surrogate model with larger motions (discussed in the following section), a more energetic sea-state is run for the same wind speed ($U_{\text{mean}} = 11$ m/s) and turbulence intensity (TI=15%). For this more energetic sea-state, H_s is 10 m and T_p is 16.5 s. This sea-state is run for the controller turned off and also for the controller turned on. Finally, it is also found that when training the surrogate model for Case 4 (benign sea sate with rated wind speed with turbulent wind and the turbine controller turned on), a higher turbulence

TABLE 1 | Wind and sea-state environmental conditions and controller activation status for the eight target cases (*note:* these values are at full-scale).

Case no.	Case name	U_{mean} (m/s)	TI (%)	Shear (-)	H_s (m)	T_p (s)	γ (-)	Controller status
1	Benign rated, constant wind, no controller	11	0 (constant)	0.14	1.8	9.1	1	Off
2	Benign rated, constant wind, with controller	11	0 (constant)	0.14	1.8	9.1	1	On
3	Benign rated, turbulent wind, no controller	11	15	0.14	1.8	9.1	1	Off
4	Benign rated, turbulent wind, with controller	11	15	0.14	1.8	9.1	1	On
5	50-year rated, constant wind, no controller	11	0 (constant)	0.14	5.5	9	5	Off
6	50-year rated, constant wind, with controller	11	0 (constant)	0.14	5.5	9	5	On
7	50-year rated, turbulent wind, no controller	11	15	0.14	5.5	9	5	Off
8	50-year rated, turbulent wind, with controller	11	15	0.14	5.5	9	5	On

intensity (TI=0.237) is beneficial in increasing the accuracy of the surrogate model, so this case is run in OpenFAST for that training. Note that this value of TI was chosen because it represented DLC 1.3, which models rated wind with the extreme turbulence model.

2.3 | Surrogate Model Development

In this section, the data analysis problem is formulated to train, validate and test the surrogate models.

During each OpenFAST run described above (and summarised in Table 1), 150 min are simulated. Ninety minutes of data is designated as the training data, with 30 min for validation (all at full-scale). This validation dataset is used for fine tuning of the model hyperparameters, such as the number of nodes in each layer and the number of layers in the model. Finally, 30 min of data is designated as a testing dataset from which the performance is reported.

Two types of surrogate model are considered: a MLR and an ANN. MLR and ANN methods are used as a demonstration of the methodology and to explore whether differing levels of model complexity are required for different cases. In general, a simpler surrogate model that performs equivalently well is preferable, and MLR generally represents the simplest surrogate model. ANNs were also considered as a convenient comparative pair as it was anticipated that there would be cases where the MLR architecture was insufficient to capture the complexity of the interactions that determine thrust, due to MLR's limited ability to capture nonlinearities. Therefore, for each case described in Table 1, a MLR and an ANN are developed with the same inputs. Where the MLR performs equivalently well when compared with the ANN, it is selected as the preferred model. All models are developed in Python 3.11.4, using the `sklearn` library for the MLR and the `keras` and `tensorflow` libraries to develop the ANN model.

To select and engineer the features for the surrogate models, data analysis techniques and domain-specific intuition are used. Crucially, since the aim of the surrogate model is to feed into experiments running in real time, only features that can be measured in the lab tests (i.e., position, time derivatives of position and functions thereof) or user-defined (i.e., wind speed and functions thereof) are selected as potential predictor variables.

2.3.1 | Constant Wind or Turbine Controller Turned Off

When the simulated wind series is assumed to be constant (Cases 1, 2, 5 and 6) or when the turbine controller is turned off (Cases 3 and 7), the surrogate modelling approach is different from when the simulated wind series is turbulent and the turbine controller is turned on (Cases 4 and 8). This difference arises due to the additional nonlinearity of the controller, which is found to increase the set of features required for satisfactory prediction. For Cases 1–3 and 5–7, all models are given the set of variables in Table 2 (thrust is the target value for prediction) as features.

TABLE 2 | OpenFAST outputs used in training surrogate models.

Variables	Symbol
Surge velocity (m/s)	$\dot{\xi}_1$
Heave velocity (m/s)	$\dot{\xi}_3$
Pitch velocity (deg/s)	$\dot{\xi}_5$
Pitch acceleration (deg/s^2)	$\ddot{\xi}_5$
Pitch (deg)	ξ_5
Wind speed (m/s)	u
Thrust (N)	T

All MLR models follow the general form:

$$\hat{T}(t) = \hat{\beta}_0 + \sum_{i=1}^{N} \hat{\beta}_i f_i(t) \tag{1}$$

where $\hat{T}$ is the predicted value for the thrust T at time t, $\hat{\beta}_i$ is the i_{th} regression coefficient and f_i is the i_{th} feature at time t. For Cases 1–3 and 5–7, the MLR model is described by Equation (2), where $\dot{\xi}_1$ is the surge velocity, $\dot{\xi}_3$ is the heave velocity, $\dot{\xi}_5$ is the pitch velocity, $\ddot{\xi}_5$ is the pitch acceleration, ξ_5 is the pitch position and u is the wind speed at hub-height. The regression coefficients, $\hat{\beta}_i$, are fit based on the training data using least squares minimisation.

$$\hat{T}(t) = \hat{\beta}_0 + \hat{\beta}_1\dot{\xi}_1(t) + \hat{\beta}_2\dot{\xi}_3(t) + \hat{\beta}_3\dot{\xi}_5(t) + \hat{\beta}_4\ddot{\xi}_5(t) + \hat{\beta}_5\xi_5(t) + \hat{\beta}_6 u(t) \tag{2}$$

For each ANN model developed for Cases 1–3 and 5–7, a feedforward architecture is used with six input features corresponding to each of the variables in Table 2. For these cases, ANNs are developed with five hidden layers with six nodes in each layer, which use the rectified linear unit (ReLU) activation function, that is, $a(x) = MAX(0, x)$. This architecture is selected, by trial-and-error using training and validation data, to ensure that the ANN has sufficient ability to model highly complex behaviour. The output of the network is a single linear combination of the outputs from the fifth hidden layer. To evaluate the performance of the model, a suitable error metric must be defined. For time series analysis, mean absolute percentage error (MAPE) is often used for quantifying the performance of a predictive algorithm. However, MAPE suffers from the fact that when the target value for prediction is small, the percentage error can become very large. Since the thrust force varies significantly and is sometimes very small, the error metric reported in this study is the mean absolute error over average observed thrust, as shown in Equation (3).

$$\epsilon = \frac{\sum_t |\hat{T} - T\,|}{\bar{T}} \times 100 \tag{3}$$

This essentially gives an error percentage compared to the average thrust. Coefficient of determination values (R^2) are also reported. These error metrics, for all eight target cases, are shown in Table 3.

It is found that for cases where there is no controller or where the windspeed is constant (i.e., Cases 1—3 and 5—7), the MLR model performs equivalently well as the ANN, and therefore, the MLR is the preferred model. This is illustrated by Figure 2 which shows 300 s of the training data and 300 s of the validation data for Case 1 as well as the prediction for the MLR and the ANN (for portions of both the training and validation datasets). The respective ϵ values (as defined in Equation (3)) for the MLR are 1.99 for the training data and 1.95 for the validation data, while for the ANN, they are 1.99 for the training data and 1.96 for the validation data. This represents an example of when a MLR is chosen over an ANN, since the more complex surrogate model (ANN) offers no improvement over the simpler one (MLR). As shown in Table 3, this happens for Cases 1–3 and 5–7.

As mentioned in Section 2.2, OpenFAST has a tendency for underprediction in platform response for low frequencies and for extreme waves. Therefore, if the sea-state to be tested in the lab is used in the training of the surrogate model, it is likely that the lab experiment would include larger inputs for platform motions than those seen in the training data. Consequently, the surrogate model would be forced to extrapolate, potentially leading to spurious thrusts being applied (and unrealistic responses). To

TABLE 3 | Error metrics for the surrogate models for all cases.

Case no.	Case name	Selected surrogate model	Mean thrust $\overline{T}$ (N)	Training ϵ (%)	Testing ϵ (%)	Training R^2	Testing R^2
1	Benign rated, constant wind, no controller	MLR	2.02×10^6	1.99	0.59	0.97	0.85
2	Benign rated, constant wind, with controller	MLR	2.02×10^6	0.79	0.59	0.84	0.85
3	Benign rated, turbulent wind, no controller	MLR	2.02×10^6	1.99	1.95	0.97	0.97
4	Benign rated, turbulent wind, with controller	ANN	1.60×10^6	4.59	3.73	0.92	0.95
5	50-year rated, constant wind, no controller	MLR	2.02×10^6	1.99	0.77	0.97	0.97
6	50-year rated, constant wind, with controller	MLR	1.98×10^6	1.56	0.78	0.90	0.94
7	50-year rated, turbulent wind, no controller	MLR	2.02×10^6	1.99	1.99	0.97	0.97
8	50-year rated, turbulent wind, with controller	ANN	1.76×10^6	5.9	5.27	0.85	0.88

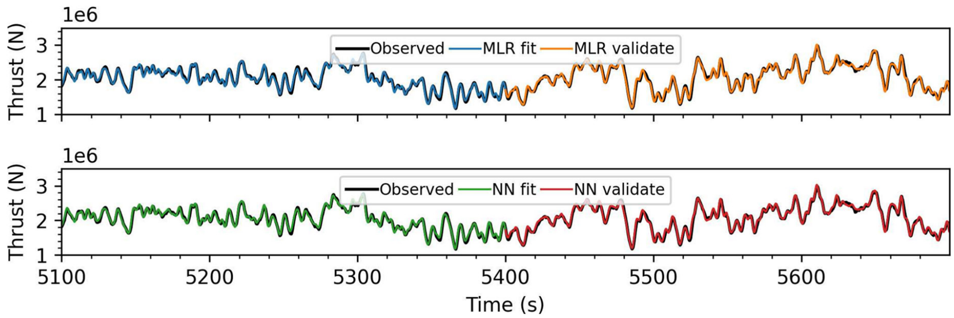

FIGURE 2 | Illustrating the performance of the MLR and ANN for thrust prediction for the benign rated case for constant wind, when the controller is switched off (Case 1 in Table 1). Both the MLR and ANN achieve satisfactory performance, and therefore, the simpler MLR is selected as the surrogate model for this case.

overcome this, for Cases 1, 3, 5, and 7 (all of the cases where the controller is turned off), the training data are a more energetic sea-state (H_s=10 m, T_p=16.5 s) with a turbulent wind input time series. For these cases, the testing error, shown in Table 3, is calculated from the OpenFAST runs for the uninflated wave conditions (H_s=5.5 m, T_p=9 s) which were run in the lab. This process explains the reduced testing error while it can be noted that the training and validation error are very similar (as described above). In real terms, the training error is very conservative compared to conditions likely in the lab, while the testing error is likely to be slightly optimistic. It is also found that a single MLR model performs equivalently well for all of the cases without the active controller, compared to making different models for each case.

For the cases when the wind is constant and the controller is turned on (Cases 2 and 6), training on a more energetic sea-state offered no improvement in predicting thrust, so the surrogate models are trained on the OpenFAST runs which directly correspond to the respective sea-state. It is speculated that this is due to the relative importance of the nonlinearity of the controller, as opposed to extreme motion response. Therefore, the key aim for the training data is to be representative of the specific wind regime in which the controller is operating.

Table 3 shows that ϵ values are $< 2\%$ for the MLR surrogate models described in this section (Cases 1–3 and 5–7). It can also be seen that the R^2 values are all high (> 0.95) for Cases 1, 3 and 5–7. The R^2 value is not as high for Case 2 (constant wind with controller), showing that the variation around the mean is not as well captured compared to assuming the mean value of thrust at all times. This is likely due to the decreased variability in thrust for constant wind with the controller turned on.

2.3.2 | Turbine Controller Turned on With Nonzero Turbulence

When the controller is turned on with nonzero turbulence intensity (Cases 4 and 8), the approach to developing an appropriate surrogate model differs. In these cases, the set of predictor features, which are summarised in Table 4, is expanded to include time history of the wind speed and indications of the different wind speed 'regimes'. These wind regimes are defined based on the ROSCO wind turbine controller [28]. Regime 1, the 'below-rated' region, is defined as $u < 9.5$ m/s, where the goal of the controller is to maximise power by changing the generator torque (and thus the rotor speed). Regime 2, the 'transition region,' is defined as $9 < u < 11$ m/s, and Regime 3, the 'above-rated' region, is defined as $u > 11$ m/s. In both of these regimes, the goal of the controller is to maintain maximum power by changing blade pitch.

Using domain knowledge and the results of incremental modifications of the set of features on the training and validation errors, the final set of features is established. It is found that features corresponding to 1-min and 10- and 1-s moving average wind speed are useful predictor variables, as well as features corresponding to the difference between the 10- and 1-s moving average wind speed according to wind speed regime. It is speculated that these features improve surrogate model performance due to the operation of the controller, which operates based on proportional, integral and derivative terms and, as described above, operates differently in each wind speed regime. It is also found that directly feeding time history for the past minute (at 40 Hz) into the neural network results improves the validation results, so this is included in the final set of features, which are summarised in Table 4.

Similar to when the controller is off, a MLR and an ANN are then trained on the set of features described in Table 4 for Cases 4 and 8, corresponding to the benign rated and 50-year rated sea-states, with turbulent wind and the turbine controller turned on. In these cases, the surrogate models are significantly more complex, since, including the time history, there are 2416 input features. Using the validation dataset to tune the model hyperparameters, it is found that a five-layer network with 15 nodes in each layer is suitable. The structure of the network is shown in Figure 3. The same structure is used for Cases 4 and 8.

For these cases, the ANN performs significantly better than the MLR, capturing more of the variation in the thrust. Figure 4

TABLE 4 | Features used for more complex wind loading cases, where $\chi_i = \begin{cases} 1, & \text{if } u \text{ is in regime } i \\ 0, & \text{otherwise} \end{cases}$.

Predictor	Description	Predictor	Description
$\dot{\xi}_1$	Surge velocity (m/s)	$< u_{60} >$	1-min moving average u (m/s)
$\dot{\xi}_3$	Heave velocity (m/s)	$< u_1 > \chi_1$	$< u_1 >$ in wind regime 1 (m/s)
$\dot{\xi}_5$	Pitch velocity (deg/s)	$< u_1 > \chi_2$	$< u_1 >$ in wind regime 2 (m/s)
$\ddot{\xi}_5$	Pitch acceleration (deg/s2)	$< u_1 > \chi_3$	$< u_1 >$ in wind regime 3 (m/s)
ξ_5	Pitch (deg)	$(< u_1 > - < u_{10} >)\chi_1$	Difference $< u_1 > - < u_{10} >$ regime 1 (m/s)
u	wind speed (m/s)	$(< u_1 > - < u_{10} >)\chi_3$	Difference $< u_1 > - < u_{10} >$ regime 2 (m/s)
$< u_1 >$	1-s moving average u (m/s)	$(< u_1 > - < u_{10} >)\chi_2$	Difference $< u_1 > - < u_{10} >$ regime 3 (m/s)
$< u_{10} >$	10-s moving average u (m/s)	$u(t) \rightarrow u(t-60)$	Last 1-min wind speed history (m/s)

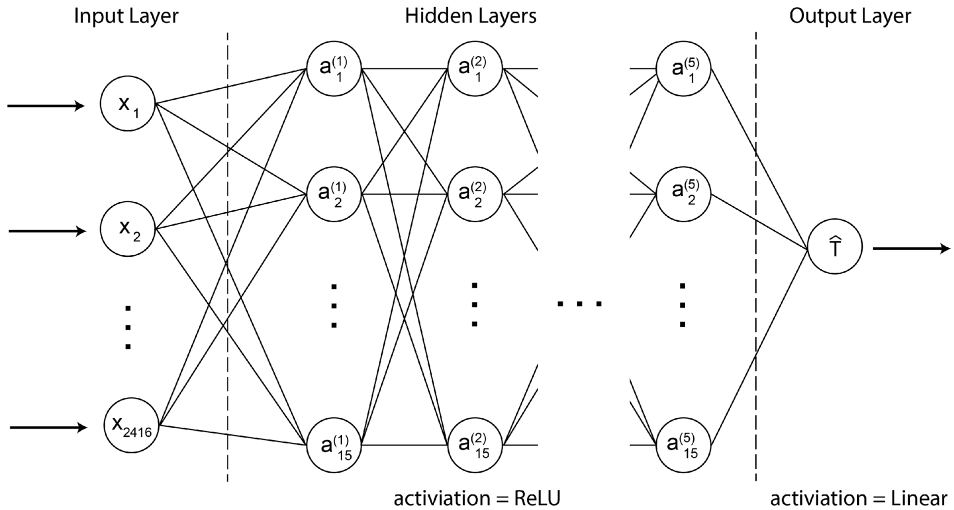

FIGURE 3 | Illustrating the structure of the ANN surrogate model for the more complex wind loading cases, when there is a turbulent wind series with the turbine controller turned on. The hidden layer nodes use the ReLU activation function, while the value for thrust prediction is a linear combination of outputs from the final hidden layer.

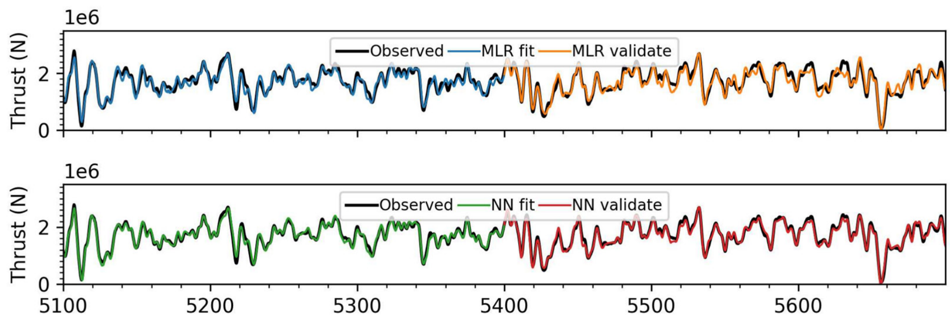

FIGURE 4 | Illustrating the performance of the MLR and ANN for thrust prediction for the benign rated case for a turbulent wind series when the controller is switched on (Case 4 in Table 1) for 300 s of the training and 300 s validation data. It can be seen that the ANN (lower plot red line) shows a better fit to the validation data (black line) when compared to the MLR (upper plot orange line).

shows 300 s of training data and 300 s of validation data for Case 4, as well as the prediction for the MLR and ANN. For this case, the MLR produces ϵ values of 7.21 on the training data and 7.27 on the validation data, while the ANN yields 4.59 for the training data and 4.46 for validation. In contrast to Cases 1–3 and 5–7, the ANN clearly offers significant improvement compared to the MLR for this case. This is also found to be true for Case 8, which is why an ANN is chosen for both of these cases.

Similar to the MLR surrogate models trained in the previous section, the ANN for Case 8 (50-year rated, turbulent wind, with the turbine controller turned on) is trained on an OpenFAST run with a more energetic sea-state (H_s=10 m, T_p=16.5 s) with a turbulent wind input time series and the turbine controller turned on. As before, this is to ensure that the training data include sufficiently large motions to reduce extrapolation, due to the known underprediction in OpenFAST. Furthermore, it is found that training Case 4 (benign rated, turbulent wind, with the turbine controller turned on) on an OpenFAST run with the same sea-state but a wind series with higher turbulence intensity (TI=0.237) resulted in a better performance on the validation data. It is speculated that this is due to an increased frequency of wind speed changes that span across different regimes within the training data. We note that an improvement in performance on the validation data could also be achieved by increasing the length of the training dataset. Taking 90 min with TI=0.15 as a benchmark, a longer training dataset (120 min) achieves an ϵ reduction of 0.3, while a higher TI (0.237) achieves an ϵ reduction of 0.5. Training with a higher TI was preferred since increasing the data length led to an ever smaller improvement and led to practical computational difficulties associated with the size of the training dataset. Using an increased TI yielded a slightly larger improvement than the longest training dataset tested, while not changing the computational requirements. The higher TI during model training explains the lower testing error than training error in Table 3.

Error metrics for the surrogate models selected for Cases 4 and 8 (benign and 50-year rated, respectively, with turbulent wind, with the turbine controller turned on) are shown in Table 3. For the testing data sets for Cases 4 and 8, respectively, ϵ values are shown to be 3.73 and 5.27 and R^2 values are shown to be 0.951 and 0.875. These error metrics are larger than for the simpler load cases due to the increased complexity of the system dynamics.

Hyperparameters for training the ANNs are shown in Table 5, and the code for the development of the ANN surrogate model

TABLE 5 | Hyperparameters for the ANN models.

Property	Value	Property	Value
Number of hidden layers	5	Training epochs	200
Number of nodes per hidden layer	15	Batch size	100
Optimiser	Adam	Learning rate	0.001
Loss	Mean squared error	Decay rates (β_1, β_2)	(0.0, 0.999)

with a demo OpenFAST file can be found on Github [31]. Once the selected machine learning models were trained, the optimal coefficients (MLR) and weights and biases (ANN) were extracted from the python models. Equivalent models were constructed in MATLAB using the extracted values, which allowed for easy integration with the existing experimental setup, as explained more in Section 3.2.

3 | Application of the Methodology to Laboratory Tests

3.1 | Laboratory Setup, Scaled Model and Instrumentation

Experiments were conducted in the Ocean Basin at the University of Plymouth's COAST laboratory. This is a 35 m long × 15.65 m wide wave basin, equipped with 24 flap multidirectional wave makers of 2.0-m hinge depth.

In this experiment, the lab-scale model was designed based on the open-source VolturnUS-S platform [18]. The scaled modelling setup is shown in detail in Figure 5a–f. Table 6 lists the geometric and mass properties.

The three-line mooring system was adapted from the 200-m mooring system designed for the VolturnUS-S by Allen et al. [18] for the shallower water depth modelled in these tests (70 m at full-scale). The top angle was designed to stay the same as the reference layout, following the approach of Pillai et al. [32], and the anchor radius was designed so that a nontruncated system would fit into the basin. The quasi-static mooring model MoorPy [33] was used to confirm that the restoring properties remained the same as for the 200 m design. Figure 5d shows a geometry schematic of the mooring chains. Table 7 summarises the mooring line properties, and Figure 6 shows the mooring layout. To achieve the target density, one extra link was attached to the chain every 920 mm, as shown in Figure 5e. Mooring line tensions were measured using FUTEK LSB210 S Beam Jr. submersible 100 lb capacity load cells, with a capture frequency of 1613 Hz. The load cell attachment to the model is shown in Figure 5f.

Three resistance type wave gauges were positioned in the lab to measure the wave conditions that the model was exposed to, as shown in Figure 6. An additional wave gauge was placed at the location of the model to calibrate the wave spectra when running tests in the empty tank (which was removed when the model was installed). Data were acquired using Edinburgh designs wave gauge controllers.

The motion of the device was recorded at a capture frequency of 128 Hz using an optical tracking system, Qualisys. Qualisys uses a set of cameras located around the Ocean Basin to track a set of reflective targets on top of the models (as shown in Figure 5b), to determine the 6 degree-of-freedom motion of the bodies. Results presented in this paper use a right-hand coordinate axis, with x being in the direction of wave propagation and z being vertical, increasing with altitude from the mean water line.

3.2 | Aerodynamic Emulation Simulation and Instrumentation

Figure 7 shows a flow chart of the RTHT method. The surrogate model takes wind speed, platform motions, velocities and accelerations and functions thereof, as inputs. During the lab tests, appropriate waves are run in the basin. Platform motions are recorded by Qualisys motion tracking system. Velocities, pitch acceleration and pitch displacement are filtered for noise, using a moving average filter. A time period of 15/128 s before the time frame of interest is analysed. The average of the time series over that time period is assigned to the middle time frame. All within the same MATLAB script, these motions are scaled up (using Froude scaling), and the surrogate model is called to obtain a requested thrust value. Thrust is scaled back down (using Froude scaling) and converted to an appropriate pulse width modulation (PWM) value. Prior to the experiments, a cantilever system (shown in Figure 5c) was used to define a calibration curve, to convert thrust force to PWM [14]. During the experiments, a single-board Nano Arduino microcontroller is then used to control the thruster to produce the requested thrust value. The thruster, as shown in Figure 5b,c consists of two drone propellers. Each side includes a T-Motor MN3510-25 360KV motor, a T-Motor Air 40A ESC 2-6S No BEC controller and a T-Motor NS (Ultra Light) Carbon Prop 14 × 4.8 propeller. The two sides contra rotate, with the starboard side rotating clockwise and the port side rotating counterclockwise. The requested thrust is then provided by the thruster and the simulation loop repeats.

3.3 | Experimental Test Campaign

Six wind loading cases were run for each of the two sea-states in the lab. In addition to the four wind loading cases described in Section 2.2 and shown in Table 1, two additional wind loading cases were tested for each of the two sea-states: (i) **No wind:** no aerodynamic emulation was used for this case (i.e., the thruster was not used) and (ii) **Constant thrust:** a constant thrust value was used for the entire run. For this latter case, the constant value of thrust used was determined by taking the average thrust value for the OpenFAST simulation corresponding to the turbulent wind series with the controller turned on for the appropriate sea-state (Case 4 for the benign sea-state and Case 8 for the 50-year rated sea-state).

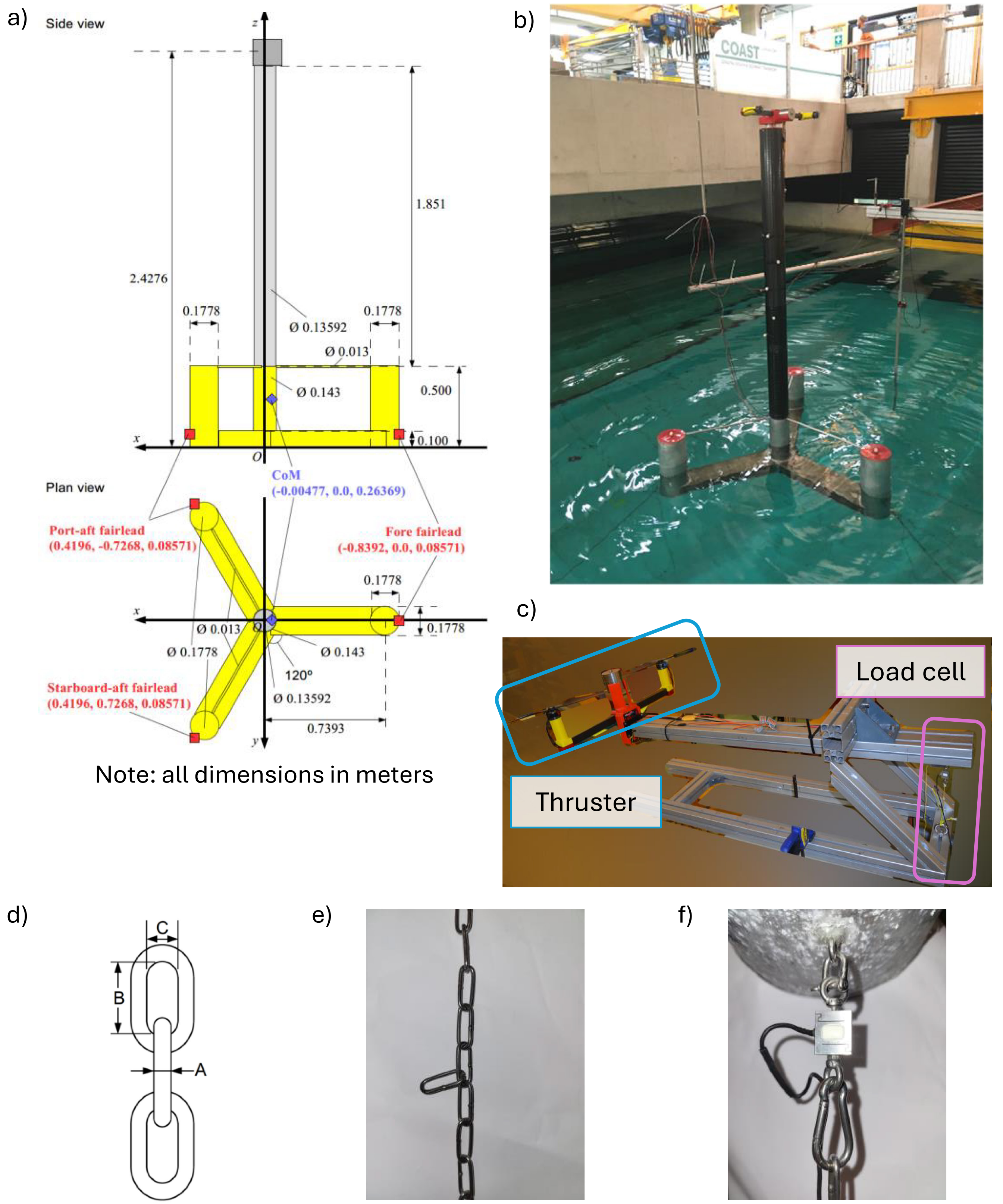

FIGURE 5 | (a) Model dimensions, definition of body-fixed coordinate system and position of CoM and mooring fairleads (in body-fixed system). (b) 1:70 scale model of the VolturnUS-S platform in the Ocean Basin at the COAST laboratory, University of Plymouth. (c) The thruster setup on a cantilever with load cell for calibration and bench tests. (d) Mooring chain geometry schematic. A, B, and C are specified in Table 7. (e) Mooring line chain, showing the extra link every 920 mm to achieve the target density. (f) The load cell attached to the model.

4 | Results

In Figure 8, the frequency-domain results for these six aerodynamic load cases for the 50-year rated case are compared, including the fore mooring line tension and the responses of the model in surge, heave and pitch modes at lab-scale. Note that these plots have been smoothed using the convolution function in Python, with window size of 10. Red shading represents the low-frequency range, and blue shading represents the wave–frequency range, and the boundary ($0.5f_p$) is denoted with a vertical dotted line. This figure shows that different aerodynamic loads result in significantly different mooring line tension and body motion responses, showing the importance of representing the correct aerodynamic loading when performing lab tests for FOWTs. As shown in Figure 8a, mooring line tension is larger when there is aerodynamic loading. At very low frequencies, the turbulent wind cases show larger mooring line tension than the constant wind cases, and at frequenices around the cut-off for low- and wave-frequencies, turbulent wind results in larger mooring line tension. As shown in Figure 8b, the surge natural frequency for the no wind case (approximately 0.07 Hz) is different than for all of the other cases with aerodynamic load (for which it is approximately 0.15 Hz). Furthermore, at the lowest frequencies, both turbulent wind cases result in larger motion amplitudes, and at frequencies around 0.2–0.6 Hz, turbulent wind with the controller on results in larger amplitudes than all the other load cases. For the remainder of the wave–frequency range, the aerodynamic load has little effect on surge response. As shown in Figure 8c, heave response is not very sensitive to aerodynamic loading, which is expected. Finally, as shown in Figure 8d, pitch response is very sensitive to aerodynamic loading: turbulent wind results in larger pitch motion response, especially when the controller is turned on, for all frequencies below 0.8 Hz.

TABLE 6 | Model dimensions and mass properties.

Property	Value (at lab-scale)
Diameter of central column	0.143 m
Diameter of outer columns	0.178 m
Height of columns	0.500 m
Distance between central and outer column axes	0.739 m
Width of pontoons	0.178 m
Depth of pontoons	0.100 m
Mass	56.3 kg
CoM position (x, y, z)	(−0.005, 0.0, 0.264) m
I_{xx}	26.68 kg m^2
I_{yy}	26.68 kg m^2
I_{zz}	14.18 kg m^2

Note: Note that (x, y, z) coordinates are given with respect to the centre bottom of the model.

In Figure 9, the frequency-domain results for the six aerodynamic load cases for the benign rated case are compared, including the mooring line tension and the responses of the model in surge, heave and pitch modes at lab-scale. Note that these plots have also been smoothed using the convolution function in Python, with window size of 10. This figure shows similar general trends to the 50-year rated results (Figure 8), but the influence of the aerodynamic load is even more prevalent for this sea-state, since the waves are smaller and thus have a smaller relative influence. In particular, as shown in Figure 9a, at low frequencies, the mooring line tension for turbulent wind with the controller on has the largest tension,

TABLE 7 | Mooring line properties for the three-line mooring setup.

Property	Value (at lab-scale)
Dry density of mooring lines	0.138 kg/m
Fore fairlead position (x, y, z)	(−0.839, 0.000, 0.086) m
Starboard-aft fairlead position (x, y, z)	(0.420, −0.727, 0.086) m
Port-aft fairlead position (x, y, z)	(0.420, 0.727, 0.086) m
Anchor radius	6.857 m
Mooring line stretched length	6.437 m
Fore anchor location (x, y, z)	(−6.857, 0.000, −1.000) m
Starboard-aft anchor location (x, y, z)	(3.429, 5.939, −1.000) m
Port-aft anchor location (x, y, z)	(3.429, −5.939, −1.000) m
Bar diameter (A in Figure 5d)	0.00282 m
B in Figure 5d	0.0263 m
C in Figure 5d	0.0065 m

Note: Note that (x, y, z) coordinates of fairlead positions are given with respect to the centre of the model, and (x, y, z) coordinates of anchor locations are given with respect to the.

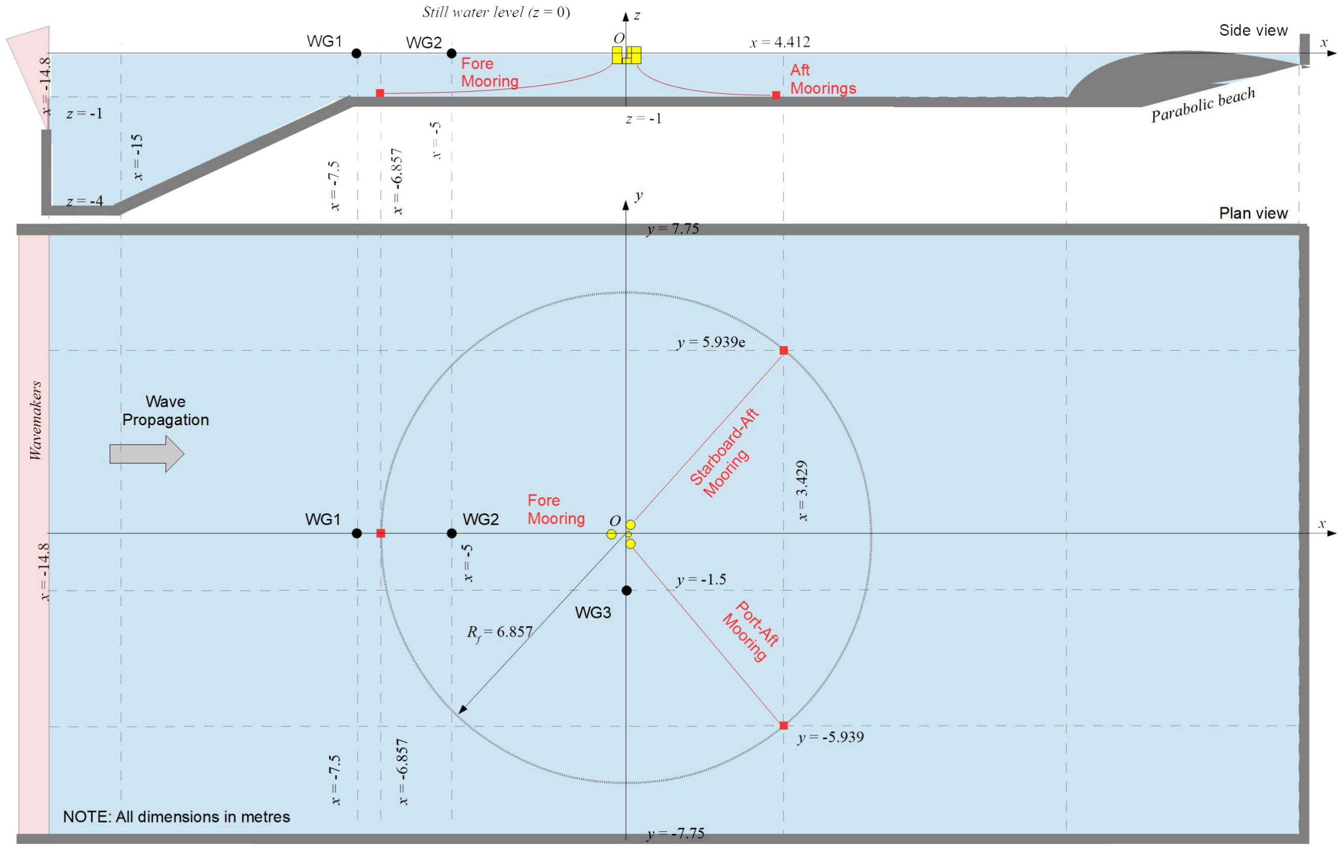

FIGURE 6 | Mooring layout for the three-line mooring setup in the laboratory, including side view (top) and top view (bottom). 'WG1,' 'WG2,' and 'WG3' correspond to the three wave gauges. Red dots correspond to anchor locations, and red lines correspond to mooring lines. The yellow floating body represents the model.

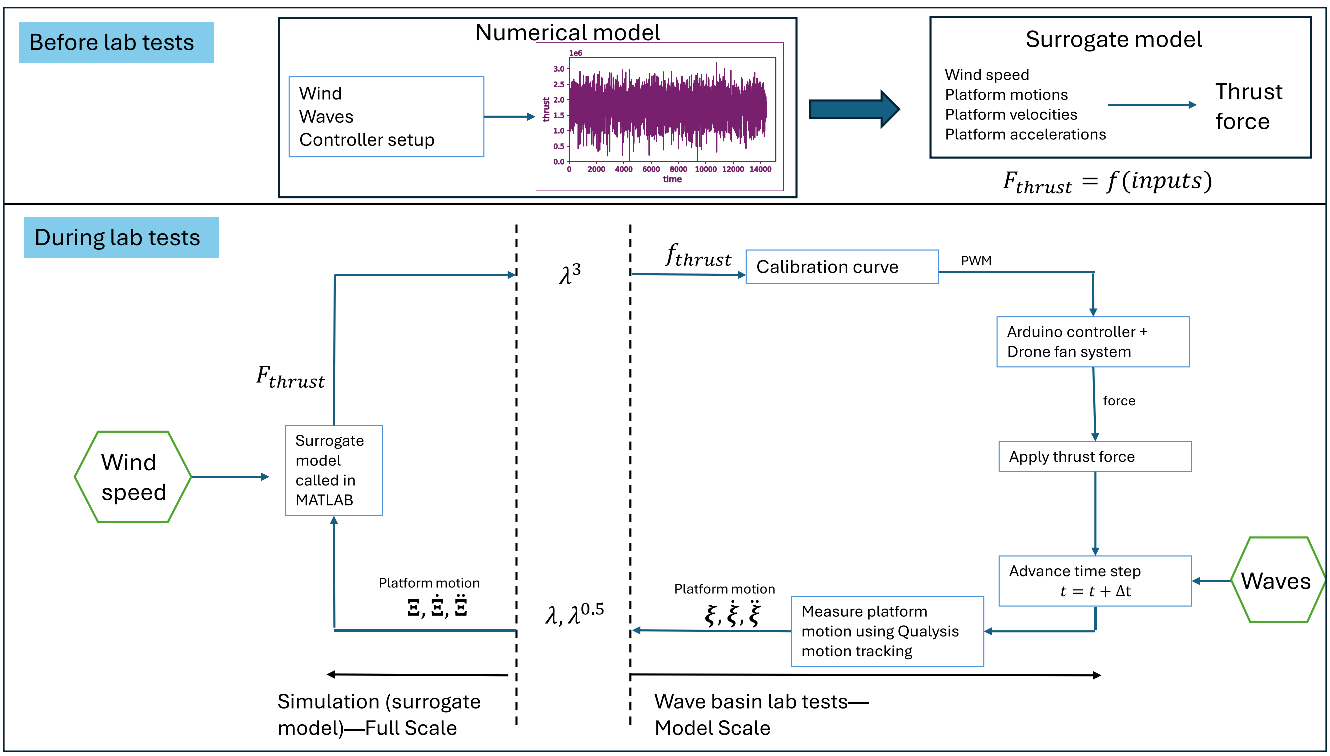

FIGURE 7 | Flow diagram of the RTHT method using a surrogate model for aerodynamic emulation.

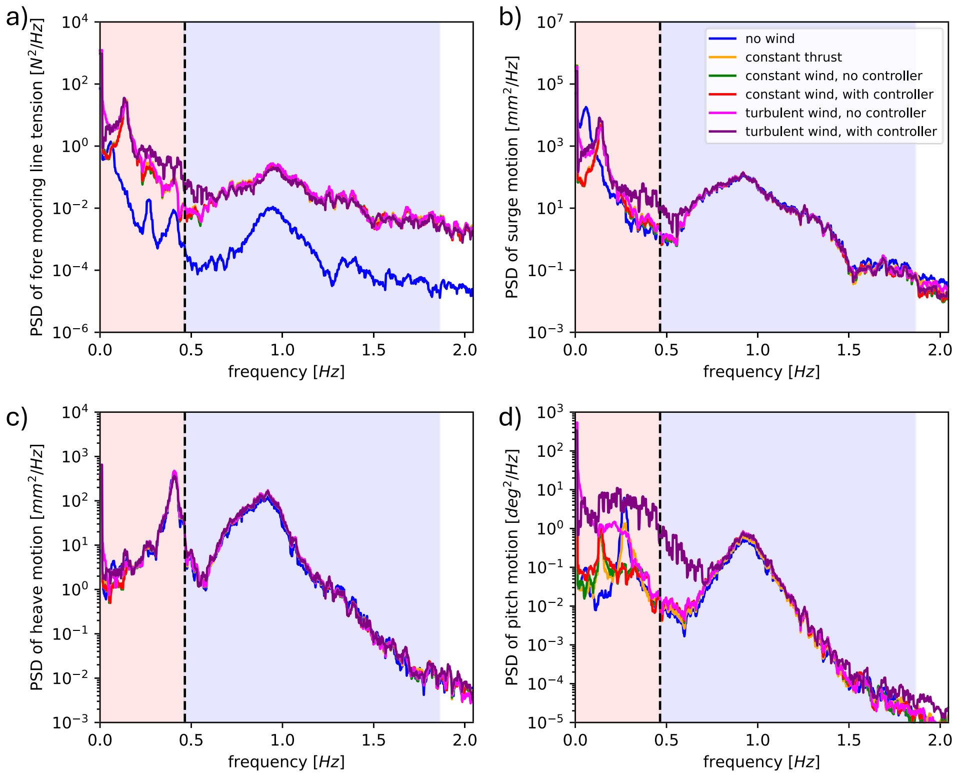

FIGURE 8 | Frequency-domain power spectral density plots for all six wind load cases for the '50-year rated' case: (a) fore mooring line tension, (b) surge response, (c) heave response and (d) pitch response. Red shading represents the low-frequency range, and blue shading represents the wave–frequency range. Note that results are shown at lab-scale.

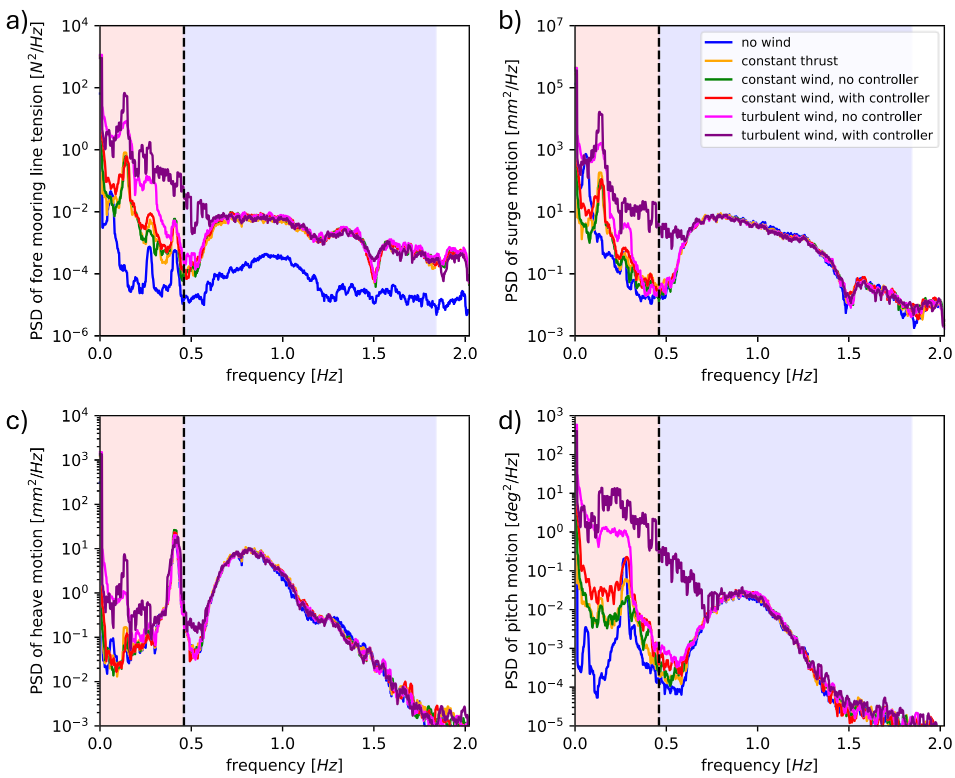

FIGURE 9 | Frequency-domain power spectral density plots for all six wind load cases for the 'benign rated' case: (a) fore mooring line tension, (b) surge response, (c) heave response and (d) pitch response. Red shading represents the low-frequency range, and blue shading represents the wave–frequency range. Note that results are shown at lab-scale.

followed by turbulent wind with no controller, then the constant wind cases, and the no-wind case has the smallest mooring line tension. Similarly, as shown in Figure 9b, the surge response is larger for turbulent wind for all low frequencies. In contrast to the 50-year rated case, as shown in Figure 9c, the heave response changes with the aerodynamic load for the benign sea-state: For turbulent wind, it is larger than for the other wind load cases in low frequencies. Figure 9d shows that pitch response is even more sensitive to aerodynamic load for the benign sea-state than for the 50-year rated case (Figure 8d). In particular, pitch response is much larger for turbulent wind, compared to the other wind cases.

4.1 | Uncertainties and Error Propagation

The measured values of position of the floating platform (as measured with Qualisys) are subject to positional uncertainties, which propagate through the surrogate model. The uncertainty is reported via the Qualisys calibration file, which gives a translational positional uncertainty (measured as the standard deviation of the T-shaped wand length) of σ_t=0.488 mm in this experimental setup. To find the rotational uncertainty, it is assumed that the translational uncertainty is the same perpendicular to the T-shaped wand, and the angle to the maximum perpendicular displacement is calculated to be σ_r=0.047° (for a 60 cm wand). Using these values, the uncertainties can be calculated for the measurements input into the surrogate models. Since a moving average filter is used, the uncertainties of displacements are $\sigma_{\xi_i} = \sigma_t/\sqrt{15}$ (for i=1,3) and $\sigma_{\xi_i} = \sigma_r/\sqrt{15}$ (for i=5). The uncertainties of velocities are $\sigma_{\dot{\xi}_i} = \sqrt{2}\sigma_{\xi_i}$, and for accelerations, it is $\sigma_{\ddot{\xi}_i} = \sqrt{2}\sigma_{\dot{\xi}_i}$. We note that there is no uncertainty in the windspeed since this is specified, not measured.

The uncertainty in the MLR models can then be calculated based on the weights (β_i, as defined in equation 1) as follows:

$$\sigma_{MLR} = \sqrt{(\beta_{\xi_5}\sigma_{\xi_5})^2 + (\beta_{\dot{\xi}_5}\sigma_{\dot{\xi}_5})^2 + (\beta_{\ddot{\xi}_5}\sigma_{\ddot{\xi}_5})^2 + (\beta_{\dot{\xi}_1}\sigma_{\dot{\xi}_1})^2 + (\beta_{\dot{\xi}_3}\sigma_{\dot{\xi}_3})^2} \tag{4}$$

For the MLR used in Case 1, this leads to an uncertainty for the MLR of σ_{MLR}=1746 N (0.08% of the average thrust). For the ANN models, the propagation of uncertainty is less straightforward. To understand the uncertainty in the predicted thrust associated with the ANN, noise is randomly added in the range $[-\Delta, +\Delta]$, where Δ is the uncertainty associated with the relevant input feature (i.e., pitch, surge velocity, heave velocity, pitch velocity and pitch acceleration). This procedure is run 100 times for the ANN for Case 4, which resulted in an uncertainty of σ_{ANN}=20,035 N (1% of the average thrust). Therefore, it is concluded that the impact of uncertainty in the measured values by Qualisys has relatively little impact on the surrogate model.

5 | Discussion

A fundamental limitation with the RTHT method is that the accuracy of the method is limited by the accuracy of the numerical model. In this study, OpenFAST is used, which is a coupled aero-hydro-servo-elastic numerical model in the time domain designed to model offshore wind turbines. Within the aerodynamic module, AeroDyn, a blade-element/momentum (BEM) algorithm is used to calculate aerodynamic thrust, with corrections such as tip-loss and hub-loss models, Glauert's correction, unsteady aerofoil aerodynamics, potential flow-based tower influence, and Pitt/Peter's skewed wake model [34]. While widely used in industry and academic research and very efficient computationally, BEM is an approximate model with limitations in accuracy for certain applications (e.g., radial flow and stalled conditions). While OpenFAST is used here as a proof-of-concept, the purpose of developing this surrogate-model-based method is to enable higher fidelity models (e.g., computational fluid dynamics, actuator line method) or experimental or field data to be used in the future.

Another limitation within OpenFAST is due to the similarly low-order hydrodynamic model. This model is a potential flow-based time domain hydrodynamic model using Cummin's equation with Morison corrections for viscous damping [35]. As discussed in Robertson et al. [36], Robertson et al. [30], and Holcombe et al. [29], this model works well for operational sea-states, but for extreme sea-states there is an underprediction of motion, especially in surge and pitch at low frequencies. In the RTHT method discussed in this paper, the accuracy of the hydrodynamics is not as crucial as the aerodynamic part of the numerical model, since in the laboratory experiments the responses will be directly determined by the scaled waves. However, the underprediction of the responses affects the training data set and thus the range of input parameters. To reduce the effect of this limitation, more energetic sea-states are used in the numerical model to train the surrogate model than those tested in the experiments, as explained in Section 2.

The other potential source of error for the RTHT method would be due to any inability of the thruster to produce requested thrust values. To quantify this error, bench tests were done after the main experiments in the wave basin, such that the thruster setup was assembled on a cantilever arrangement (the same arrangement used in calibrating the thruster setup, as described in Section 3.2 and shown in Figure 5c) with a load cell to measure the force. In these bench tests, the time series of requested thrust values recorded during the experiments described in Section 3.3 corresponding to the 50-year rated sea-state with aerodynamic loading using the surrogate models (Cases 5–8 from Table 1) were re-run while the thruster was in the cantilever setup. The force from the load cell was recorded and compared to the requested thrust time series.

Figure 10 shows samples of the comparisons between measured and requested thrust for the four cases. It can be seen that there is a time lag from the requested thrust (cyan) to the measured thrust (dark blue, shown filtered and resampled in purple). Despite this, it is shown that for the first three cases (a, b and c, corresponding to constant wind with no controller, Case 5, constant wind with the controller, Case 6, and turbulent wind with no controller, Case 7), the magnitudes of the measured thrust values seem to be consistent with the requested thrust values. However, for the final case (d, corresponding to turbulent wind with controller, Case 8), the magnitudes of the peaks and, in particular, the troughs in the measured thrust do not correspond as well with those from the requested thrust, as indicated by the black circles in Figure 10d.

To quantify the discrepancy in measured and requested thrust, ϵ (defined in Equation (3)) is used. The ϵ values for each case are summarised in Table 8. The time lag between requested and measured thrust is calculated to be between 0.204 and 0.209 s. To remove the effect of this time lag, the ϵ calculation is repeated when the measured thrust values are shifted by 0.208 s, and this is also shown in Table 8. It can be seen from this table that for the first three cases, the ϵ value is less than 2% when the time shift is accounted for and less than 5% when it is not. For the fourth case (turbulent wind with controller), the ϵ is 3.7% when the time shift is accounted for but 14.54% when it is not. The calculated errors illustrate that the latency of the system is the main source of error in the lab setup and particularly affects the final case (turbulent wind, with controller). While most RTHT method studies show a calibration curve for thrust, many do not look at how well the thruster is able to produce the actual requested thrust time series for lab tests, but this analysis clearly shows the importance of calculating this error.

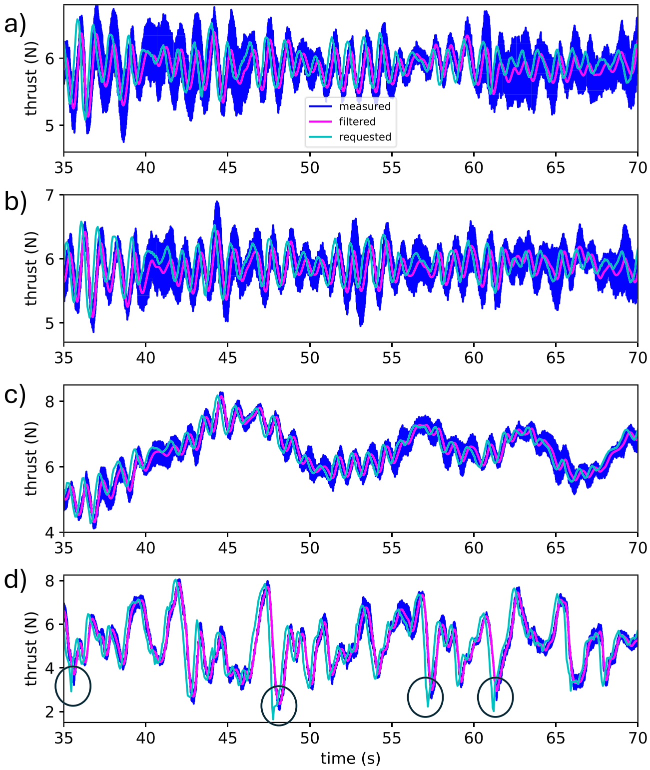

FIGURE 10 | Comparison of requested (cyan), measured (dark blue), and filtered measured (purple) thrust time series for the 50-year rated case for (a) constant wind, no controller (Case 5), (b) constant wind, with controller (Case 6), (c) turbulent wind, no controller (Case 7) and (d) turbulent wind, with controller (Case 8). Note that results are shown at lab-scale and note the different y-axis ranges.

TABLE 8 | Comparison of requested vs. measured values of thrust for the post-experiment bench tests for the 50-year rated environmental condition. ϵ, as defined in Equation (3), is shown for the four wind cases.

Case no.	Case description	ϵ (%)	ϵ with 0.208 s time shift [%]
4	Constant wind, no controller	4.44	1.84
5	Constant wind, with controller	4.34	1.28
6	Turbulent wind, no controller	4.30	1.22
7	Turbulent wind, with controller	14.54	3.70

DLC 1.1 and 1.6 (defined in Table 1) are considered in this study. These DLCs were chosen because they are crucial cases to consider when looking to certify a FOWT platform design, and they are also the most challenging to accurately capture with a surrogate model due to nonlinearities of the controller near rated wind speed. Other wind speeds are easier to capture with a surrogate model when the controller operates within a single wind regime.

In post-lab analysis, it was discovered that some of the surrogate model parameters exceeded the prescribed limits from training data used from OpenFAST simulations. The minimum pitch (negative) acceleration was below the minimum limit from the training data for Cases 4 and 6. The maximum pitch (positive) acceleration exceeded the maximum from the training data for Cases 4, 5, 6 and 8. The maximum heave velocity exceeded the maximum from the training data for Case 5, and the maximum pitch displacement exceeded the maximum from the training data for Case 3. In each experimental run, the limits were only exceeded once. In future, the training data should be even more conservative than the numerical runs performed for this study, as the experimental pitch acceleration tends to be larger than OpenFAST predicts. This phenomena should be studied further to understand the reason for the mismatch in pitch acceleration in numerical vs. experimental simulations, despite the larger sea-state for the training data.

In this study, aerodynamic thrust force was emulated in the lab, but no other components of aerodynamic load (e.g., rotor torque, gyroscopic momentum and 3P tower loading) are modelled. Thrust force is the component of the load that most directly influences platform motion, and thus, this is the load component of interest and focus for most RTHT studies [5]. However, an extension of this work would be to build a setup which can emulate other aerodynamic load components (i.e., a multipropeller actuator). It is anticipated that these other aerodynamic load components will be more easily captured with a surrogate model since the controller mostly affects the thrust force.

6 | Conclusion

In this paper, a methodology is presented for scaled physical modelling of FOWTs in a wave basin using a RTHT method. Before the lab tests, the numerical model OpenFAST is run for the VolturnUS-S semi-submersible platform with the 15MW IEA turbine. Two different types of surrogate models are developed, MLR and ANN, depending on the complexity of the wind loading. These surrogate models are trained on corresponding numerical model results to enable prediction of aerodynamic thrust from parameters that are measurable in the lab (including platform motions, velocities and accelerations) and/or user-defined (including wind speed and wind speed history). It is found that for constant wind or turbulent wind with no active turbine controller, MLRs are satisfactory surrogate models for aerodynamic thrust. For these cases, the maximum error is < 2%, and ANNs perform no better. For turbulent wind with active turbine control, ANNs are shown to improve accuracy compared to MLRs. For these case, the maximum error is < 6% for the most extreme conditions.

The methodology was demonstrated in the Ocean Basin at the COAST Laboratory at the University of Plymouth, using a 1:70 scaled model of the VolturnUS-S. Environmental conditions from the Celtic Sea, off the coast of Southwest United Kingdom, were tested. Benign operational (DLC 1.1) and 1-in-50-year (DLC 1.6) conditions for rated wind speed are investigated. Frequency-domain results of mooring line tension and surge, heave and pitch platform response are presented and discussed. It is found that different wind loading cases result in significantly different responses in both benign (operational) and extreme (1-in-50-year storm) sea-states, emphasising the importance of accurately representing aerodynamic load in RTHT methods. After the tests were completed, a cantilever setup was used to compare requested and measured thrust values. While it was found that the setup was able to produce the magnitude of the requested thrust to within 5% for most cases, the latency (0.208 s) between requested and measured thrust was shown to be a major source of experimental error for the final case (extreme sea-state, turbulent wind, with controller). Without the latency, the errors are less than 4% for all cases. It is therefore recommended that future studies using the RTHT method directly compare error in experimental requested thrust time series and work to improve latency.

While the methodology has been demonstrated in this paper, there is room for improvement in the future. It is possible that the surrogate model approach could be improved by (i) calling the turbine controller in real time, which would allow for simpler MLRs to be used for accurate thrust prediction and (ii) exploring the ANN for further enhancements which may better represent the system. The latter could include further exploration and optimisation of the input features or using a different ANN architecture (e.g., LSTMs are generally well-suited to time series problems [37]). Furthermore, more accurate underlying numerical models could also be used. OpenFAST is used in this proof-of-concept study; however, in the future a higher fidelity numerical model (e.g., computational fluid dynamics), experimental wind tunnel tests, or field data could be used to improve accuracy of the surrogate model training data. Finally, a key improvement is the development of software and/or hardware to reduce the latency for the thruster setup.

Acknowledgements

This study has been produced under the resources of the Cornwall FLOW Accelerator Project, which is led by Celtic Sea Power and delivered in partnership with the University of Plymouth, the University of Exeter and the Offshore Renewable Energy (ORE) Catapult. The Cornwall FLOW Accelerator Project has been supported by a grant from the European Regional Development Fund, project number O5R19P03188. The authors gratefully acknowledge that this work was partly funded by the Engineering and Physical Sciences Research Council, UK, through the 'Supergen ORE Hub' grant (EP/S000747/1), and 'Extreme Loading on Floating Offshore Wind Turbines (FOWTs) under Complex Environmental Conditions' grant (EP/T004177/1).

Conflicts of Interest

The authors declare no conflicts of interest.

Data Availability Statement

The data that support the findings of this study are available from the corresponding author upon reasonable request.

Peer Review

The peer review history for this article is available at https://publons.com/publon/10.1002/we.70052.

References

1. Global Wind Energy Council, "Global Offshore Wind Report 2022"; (2022), https://gwec.net/wp-content/uploads/2022/06/GWEC-Offshore-2022_update.pdf.

2. Global Wind Energy Council, "Global Offshore Wind Report 2023"; 2023, https://gwec.net/globalwindreport2023/.

3. E. C. Edwards, A. Holcombe, S. Brown, E. Ransley, M. Hann, and D. Greaves, "Evolution of Floating Offshore Wind Platforms: A Review of At-Sea Devices," *Renewable and Sustainable Energy Reviews* 183 (2023): 113416.

4. E. C. Edwards, A. Holcombe, S. Brown, E. Ransley, M. Hann, and D. Greaves, "Trends in Floating Offshore Wind Platforms: A Review of Early-Stage Devices," *Renewable and Sustainable Energy Reviews* 193 (2024): 114271.

5. A. Otter, J. Murphy, V. Pakrashi, A. Robertson, and C. Desmond, "A Review of Modelling Techniques for Floating Offshore Wind Turbines," *Wind Energy* 25, no. 5 (2022): 831–857.

6. B. Skaare, T. D. Hanson, F. G. Nielsen, R. Yttervik, A. M. Hansen, K. Thomsen, et al., "Integrated Dynamic Analysis of Floating Offshore Wind Turbines". In: European wind energy conference and exhibition, vol. 3 Hamburg, Germany; 2007. p. 1929–1939.

7. S. M. Mortensen, K. Laugesen, J. K. Jensen, K. Jessen, and M. Soltani, "Experimental Verification of the Hydro-Elastic Model of a Scaled Floating Offshore Wind Turbine," in *2018 IEEE Conference on Control Technology and Applications (CCTA)* (IEEE, 2018): 1623–1630.

8. A. J. Goupee, B. J. Koo, R. W. Kimball, K. F. Lambrakos, and H. J. Dagher, "Experimental Comparison of Three Floating Wind Turbine Concepts," *Journal of Offshore Mechanics and Arctic Engineering* 136, no. 2 (2014): 020906.

9. H. Bredmose, F. Lemmer, M. Borg, et al., "The Triple Spar Campaign: Model Tests of a 10MW Floating Wind Turbine With Waves, Wind and Pitch Control," *Energy Procedia* 137 (2017): 58–76.

10. J. Azcona, F. Bouchotrouch, M. González, et al., *Aerodynamic Thrust Modelling in Wave Tank Tests of Offshore Floating Wind Turbines Using a Ducted Fan. Journal of Physics: Conference Series*, vol. 524 (IOP Publishing, 2014): 012089.

11. T. Sauder, V. Chabaud, M. Thys, E. E. Bachynski, and L. O. Sæther, "Real-Time Hybrid Model Testing of a Braceless Semi-Submersible Wind Turbine: Part I. The Hybrid Approach," in *International Conference on Offshore Mechanics and Arctic Engineering*, vol. 49972 (American Society of Mechanical Engineers, 2016) p. V006T09A039.

12. A. Otter, J. Murphy, and C. Desmond, *Emulating Aerodynamic Forces and Moments for Hybrid Testing of Floating Wind Turbine Models. Journal of Physics: Conference Series*, vol. 1618 (IOP Publishing, 2020): 032022.

13. A. M. Urbán and R. Guanche, “Wind Turbine Aerodynamics Scale-Modeling for Floating Offshore Wind Platform Testing,” *Journal of Wind Engineering and Industrial Aerodynamics* 186 (2019): 49–57.

14. E. J. Ransley, S. A. Brown, E. C. Edwards, et al., “Real-Time Hybrid Testing of a Floating Offshore Wind Turbine Using a Surrogate-Based Aerodynamic Emulator,” *ASME Open Journal of Engineering* (2023): 2, https://doi.org/10.1115/IOWTC2022-98642.

15. G. Sun and S. Wang, “A Review of the Artificial Neural Network Surrogate Modeling in Aerodynamic Design,” *Proceedings of the Institution of Mechanical Engineers, Part G: Journal of Aerospace Engineering* 233, no. 16 (2019): 5863–5872.

16. J. Zhang, X. Zhao, D. Greave, and S. Jin, “Modeling of a Hinged-Raft Wave Energy Converter via Deep Operator Learning and Wave Tank Experiments,” *Applied Energy* 341 (2023): 121072.

17. OpenFAST, “OpenFAST v3.4.1;. Accessed: 2023-04-05, https://github.com/OpenFAST/openfast.

18. C. Allen, A. Viscelli, H. Dagher, A. Goupee, E. Gaertner, N. Abbas, et al., “Definition of the UMaine VolturnUS-S reference Platform Developed for the IEA wind 15-Megawatt Offshore Reference Wind Turbine. National Renewable Energy Lab.(NREL), Golden, CO (United States); Univ. of”; (2020).

19. E. Gaertner, J. Rinker, L. Sethuraman, F. Zahle, B. Anderson, G. Barter, et al., “Definition of the IEA 15-Megawatt Offshore Reference Wind Turbine”, (2020).

20. IEC, *Wind Energy Generation Systems – Part 3-1: Design Requirements for Fixed Offshore Wind Turbines* (IEC, 2019).

21. The Crown Estate, “Floating Offshore Wind Leasing Round 5”; 2022. https://www.thecrownestate.co.uk/en-gb/what-we-do/on-the-seabed/floating-offshore-wind/, accessed 30-08-23.

22. H. Hersbach, B. Bell, P. Berrisford, et al., “The ERA5 Global Reanalysis,” *Quarterly Journal of the Royal Meteorological Society* 146, no. 730 (2020): 1999–2049.

23. E. Mackay and G. de Hauteclocque, “Model-Free Environmental Contours in Higher Dimensions,” *Ocean Engineering* 273 (2023): 113959.

24. IEC, *Wind Energy Generation Systems – Part 1: Design Requirements* (IEC, 2018).

25. IEAWindTask37, “IEA-15-240-RWT v1.1”;. Accessed: 2023-04-05, https://github.com/IEAWindTask37/IEA-15-240-RWT.

26. G. Jeans, “Converging Profile Relationships for Offshore Wind Speed and Turbulence Intensity,” *Wind Energy Science* 9, no. 10 (2024): 2001–2015.

27. T. Burton, N. Jenkins, D. Sharpe, and E. Bossanyi, *Wind Energy Handbook* (John Wiley & Sons, 2011).

28. N. Abbas, D. Zalkind, L. Pao, and A. Wright, “A Reference Open-Source Controller for Fixed and Floating Offshore Wind Turbines,” *Wind Energy Science Discussions* 2021 (2021): 1–33.

29. A. Holcombe, E. Edwards, T. Tosdevin, D. Greaves, M. Hann, “A Comparative Study of Potential-Flow-Based Numerical Models to Experimental Tests of a Semi-Submersible Floating Wind Turbine Platform”. In: ISOPE International Ocean and Polar Engineering Conference ISOPE; 2023. p. ISOPE–I.

30. A. N. Robertson, S. Gueydon, E. Bachynski, et al., *OC6 Phase I: Investigating the Underprediction of Low-Frequency Hydrodynamic Loads and Responses of a Floating Wind Turbine. In: Journal of Physics: Conference Series*, vol. 1618 (IOP Publishing, 2020): 032033.

31. E. Barbour, “Developing a Surrogate Model Based on OpenFAST Data for Software in the Loop (SiL)”;. Accessed: 2024-04-11, https://github.com/EdwardBarbour/Surrogate_model_SiL.

32. A. Pillai, T. Gordelier, P. Thies, et al., “Anchor Loads for Shallow Water Mooring of a 15 MW Floating Wind Turbine. Part I: Chain Catenary Moorings for Single and Shared Anchor Scenarios,” *Ocean Engineering* 266 (2022): 111816.

33. M. Hall, S. Housner, S. Sirnivas, and S. Wilson, *Moorpy (Quasi-Static Mooring Analysis in Python)*National Renewable Energy Lab.(NREL), (2021).

34. P. J. Moriarty and A. C. Hansen, *AeroDyn Theory Manual* National Renewable Energy Lab, (2005).

35. J. M. Jonkman, A. Robertson, and G. J. Hayman, *HydroDyn Users Guide and Theory Manual* National Renewable Energy Laboratory, (2014).

36. A. N. Robertson, F. Wendt, J. M. Jonkman, et al., “OC5 Project Phase II: Validation of Global Loads of the Deep C Wind Floating Semisubmersible Wind Turbine,” *Energy Procedia* 137 (2017): 38–57.

37. S. Siami-Namini, N. Tavakoli, and A. S. Namin, “A Comparison of ARIMA and LSTM in Forecasting Time Series,” in *In: 2018 17th IEEE International Conference on Machine Learning and Applications (ICMLA)* (IEEE, 2018): 1394–1401.